Hyeon Seok Rou, Giuseppe Thadeu Freitas de Abreu, Junil Choi, David González G., Marios Kountouris, Yong Liang Guan, and Osvaldo Gonsa

From Orthogonal Time–Frequency Space to Affine Frequency-Division Multiplexing

A comparative study of next-generation waveforms for integrated sensing and communications in doubly dispersive channels

©SHUTTERSTOCK.COM/CINEMANIKOR

Next-generation wireless systems will offer integrated sensing and communications (ISAC) functionalities not only in order to enable new applications but also as a means to mitigate challenges, such as doubly dispersive channels, which arise in high-mobility scenarios and/or at millimeter-wave (mm-wave) and terahertz (THz) bands. An emerging approach to accomplish these goals is the design of new waveforms, which draw from the inherent relationship between the doubly dispersive nature of time-variant (TV) channels and the environmental features of scatterers manifested in the form of multipath delays and Doppler shifts. Examples of such waveforms are the delay–Doppler-domain orthogonal time–frequency space (OTFS) and the recently proposed chirp-domain affine frequency-division multiplexing (AFDM), both of which seek to simultaneously combat the detrimental effects of double selectivity and exploit them for the estimation (or sensing) of environmental information. This article aims to provide a consolidated and comprehensive overview of the signal processing techniques required to support reliable ISAC over doubly dispersive channels in beyond 5G (B5G)/6G systems, with an emphasis on OTFS and AFDM waveforms, as those, together with the traditional orthogonal frequency-division multiplexing (OFDM) waveform, suffice to elaborate on the most relevant properties of the trend. The analysis shows that OTFS and AFDM indeed enable significantly improved robustness against intercarrier interference (ICI) arising from Doppler shifts compared to OFDM. In addition, the inherent delay–Doppler-domain orthogonality of the OTFS and AFDM effective channels is found to provide significant advantages for the design and the performance of integrated sensing functionalities.

Introduction

It is expected that B5G and 6G wireless systems will employ extremely high-frequency (EHF) technologies, operating in the mm-wave and THz bands [1], as a means to support applications [2] such as the Internet of Things, edge computing, and smart cities and scenarios such as vehicle-to-everything (V2X) technology, high-speed rail, and nonterrestrial networks,

Digital Object Identifier 10.1109/MSP.2024.3422653
Date of current version: 21 November 2024

which are often subjected to heterogeneous and high-mobility conditions [3]. High-mobility scenarios are known to pose a significant challenge to wireless communications systems, due to the resulting doubly dispersive wireless channel, also referred to as *TV multipath* or *time–frequency selectivity* [4]. Such heterogeneous scattering environments deteriorate the received signal in the form of path delays and Doppler shifts, resulting in intersymbol interference (ISI) and ICI, which can drastically decrease communication performance under conventional and highly effective modulation schemes, such as OFDM [5].

There is a growing expectation that B5G and 6G systems will offer ISAC capabilities, possibly with unified hardware and signal processing techniques.

Concomitant with this challenge, there is a growing expectation that B5G and 6G systems will offer ISAC capabilities, possibly with unified hardware and signal processing techniques [6]. In addition to providing environment perception and accurate/reliable localization information to serve the aforementioned applications, the enhancements introduced by ISAC are fundamental to improve spectrum and energy efficiency and to lower hardware costs of systems operating in high-mobility scenarios [3].

While it is difficult to foresee which of the upcoming generations/standards, i.e., B5G or 6G, will see ISAC adopted and implemented in commercial systems, the topic is one of the most intensively discussed among prestandardization fora on wireless systems in recent years, with notable examples being the 6G Smart Networks and Services Industry Association (6G-IA), where ISAC has been identified as a priority technology for its members, and the 5G Automotive Association (5GAA), where ISAC is considered an enabling technology for cellular V2X services (see https://5gaa.org/ and https://6g-ia.eu/ for additional information on 5GAA and 6G-IA, respectively). Although it is reasonable to anticipate that any form of practically deployed 5G-based ISAC will likely leverage OFDM, more specifically, cyclic prefix (CP) OFDM and DFT-spread OFDM for downlink/sidelink and uplink, respectively, but for 6G, new waveforms, such as the OTFS and AFDM, should be considered to fully enable the potential of ISAC, as investigated in this article. In fact, important standardization bodies, such as the European Telecommunications Standards Institute (ETSI) and the 3rd Generation Partnership Project (3GPP), which produce technical specifications for mobile broadband systems worldwide, have recently added ISAC to their work plans and road maps, with ETSI launching a new group dedicated to ISAC in November 2023.

In line with this trend, novel waveforms have been recently proposed which, thanks to their ability to retain symbol orthogonality under doubly dispersive conditions, are both robust to high mobility and advantageous for ISAC, as they inherently enable the estimation of environmental parameters, such as the distance and velocity of scatterer objects (i.e., delay and Doppler shifts). One of the most popular methods is OTFS signaling [7], which leverages the inverse symplectic finite Fourier transform (ISFFT) in order to modulate a 2D grid of information symbols directly in the delay–Doppler domain, gaining great attention for high-mobility B5G systems thanks to its superior performance compared to currently used waveforms, such as OFDM [8].

It is easy to show, indeed, that the full delay–Doppler representation of the channel in OTFS inherently conveys the velocity and range information of the scatterers in the form of the respective multipath delays and Doppler shifts, thus implying significant benefits in terms of ISAC. As a consequence, a plethora of OTFS-based ISAC techniques have been proposed to extract the delay and Doppler parameters of the resolvable paths directly from the channel state information (CSI), which have been shown to compete with the sensing performances of OFDM and frequency-modulated continuous-wave (FMCW) radars, with higher robustness to mobility and achievable capacity [9].

An alternative strategy to design ISAC-friendly and mobility-robust waveforms is to employ chirp-based multicarrier approaches [10]. While the chirp-domain design is attractive due to the inherent spread-spectrum property and potential for full-duplex operations, an important and common drawback of these earlier approaches is the lack of adaptability to the channel delay and Doppler spreads, which is a consequence of the nonparameterizable transforms in their design.

A more recent take on the idea, which seeks to mitigate the latter drawback, is the AFDM waveform [11], which leverages the inverse discrete affine Fourier transform (IDAFT) [12] in order to modulate information symbols into a twisted time–frequency domain, yielding the desired delay–Doppler orthogonality while maintaining the necessary flexibility. The optimizable parametrization of AFDM is further accompanied by other desirable properties, such as a full diversity guarantee and increased throughput [11], making AFDM a strong candidate for an ISAC-enabling waveform for B5G and 6G systems.

This article aims to offer a thorough analysis of the fundamentals and the future of ISAC technology in heterogeneous high-mobility scenarios, in the form of a comprehensive comparison of prominent candidate waveforms, focusing on OTFS and AFDM. The analysis reveals that the novel delay–Doppler orthogonal designs of OTFS and AFDM benefit the signal processing for both communication and sensing functionalities, advocating the integration of the two. These insights may hold significant interest and value not only for academia but also for standardization engineers across various industry verticals who are increasingly participating in the development of future generations of mobile broadband systems.

The remainder of the article is organized as follows. The fundamental system models and the required ISAC signal processing techniques for the doubly dispersive wireless channel, emphasizing the inherent transformations among time, frequency, delay, and Doppler dimensions, are described in the "Signal Processing Fundamentals of

Doubly Dispersive Channels" section. (The importance of modeling the doubly dispersive channel, especially for ISAC applications, is a highly relevant problem currently discussed in both academia and standardization [13].) In the "Signal Models of Next-Generation Waveforms" section, the signal models of the identified candidate waveforms for B5G/6G ISAC in doubly dispersive environments are consolidated, highlighting their interrelationships in terms of the multiplexing (MX) domain, transmitter structure, and the core linear canonical transform (LCT). In the "ISAC Using Next-Generation Waveforms" section, we discuss the radar sensing techniques leveraging the identified candidate waveforms in terms of the radar target detection problem (DP) and radar parameter estimation problem (EP), elaborating on signal processing techniques and solutions categorized into correlation-based methods and direct/indirect CSI-based approaches. In the "KPI-Centered Comparative Analysis" section, the candidate waveforms are compared, with a basis on different key performance indicators (KPIs) for both communications and radar sensing performances in addition to implications for hardware implementation, requirements, and potential challenges. Finally, the key insights provided by the article are summarized, and some future directions of the research are identified.

High-mobility scenarios are known to pose a significant challenge to wireless communications systems, due to the resulting doubly dispersive wireless channel.

Signal processing fundamentals of doubly dispersive channels

A long history of research on wireless communications has resulted in the identification and characterization of two fundamental and distinct types of small-scale fading effects, namely, frequency selectivity and time selectivity, also known as *time dispersion* and *frequency dispersion*, respectively. In particular, an electromagnetic signal propagated through a given path is subject to a specific path delay proportional to the total propagation distance between the transmitter and the receiver and a Doppler shift proportional to the relative velocities among the transmitter, receiver, and scatterer and the carrier frequency. (We remark that in the related literature, and, therefore, also in this article, the term *Doppler shift* is often used in a broad sense, including spectral shifts of the propagated signal resulting from phenomena other than the actual Doppler effect, such as frequency offsets and low-frequency phase noise at the local oscillators.)

In a channel with multiple distinguishable propagation paths, the different copies of the originally transmitted signal with varying time delays and Doppler shifts are superposed at the receiver, resulting in interference that impacts on the reliability and performance of the wireless communication link unless appropriate signal processing techniques are employed. In this section, we first consolidate the fundamental doubly dispersive channel model with all its representations in the time, frequency, delay, and Doppler domains, along with the associated transformation methods, followed by the corresponding signal processing mechanisms available to process the received signal by the efficient representation of the input–output relationship leveraging a circular convolution matrix.

The doubly dispersive channel model

Consider a wireless channel between a transmitter and receiver, which is modeled via P significant propagation paths, where each pth resolvable path, with $p \in \{1, \ldots, P\}$, is respectively described by a corresponding complex fading coefficient $h_p \in \mathbb{C}$, path delay $\tau_p \in [0, \tau^{\max}]$, and Doppler shift $\nu_p \in [-\nu^{\max}, +\nu^{\max}]$. The corresponding delay and Doppler spreads of such a doubly dispersive channel are characterized by the maximum delay $\tau^{\max}$ (in seconds) and the maximum Doppler shift $\pm\nu^{\max}$ (in hertz) such that the channel can be described by the linear TV (LTV) relationship between the input and the output signals. The LTV channel is most commonly represented as a TV impulse response function (TVIRF) in the time delay domain, given by

$$h(t, \tau) \triangleq \sum_{p=1}^{P} h_p \cdot e^{j2\pi\nu_p t} \cdot \delta(\tau - \tau_p) \tag{1}$$

where $j \triangleq \sqrt{-1}$ is the elementary imaginary number; t and τ denote the instantaneous time and path delay, respectively; and $\delta(x)$ is the unit impulse function defined by $\delta(x) = 1$ iff $x = 0$. (The term *LTV system* is not to be confused with linear systems with time-varying delays—i.e., systems with delay drifts, where $\tau_p(t)$—which are also commonly described as LTV. In this article, we consider only time-invariant delays, in compliance with the related literature on doubly dispersive channels, e.g., [4], [7], and [11].)

Alternatively, the TVIRF in the time delay domain can also be represented in other domains by leveraging appropriate linear transforms [12]. For example, the representation in the time–frequency domain is known as the *TV transfer function* (*TVTF*), which is obtained by a Fourier transform (FT) on the TVIRF over the delay domain; i.e.,

$$\begin{aligned} H(t, f) &\triangleq \underset{\tau \to f}{\mathcal{F}}[h(t, \tau)] = \int_{-\infty}^{+\infty} h(t,\tau) \cdot e^{-j2\pi\tau f} \, \mathrm{d}\tau \\ &= \sum_{p=1}^{P} h_p \cdot e^{j2\pi\nu_p t} \cdot e^{-j2\pi\tau_p f} \end{aligned} \tag{2}$$

where f is the instantaneous frequency and $\mathcal{F}[\cdot]$ denotes the continuous FT operator.

The TVTF in the time–frequency domain readily highlights both time and frequency dispersion effects of the channel, visible in the two fast-varying exponential terms dependent on the instantaneous time t and instantaneous frequency f, respectively, at a rate of the Doppler frequency ν_p and delay τ_p of the corresponding pth propagation path, as illustrated in Figure 1(a). Conversely, the Doppler-variant impulse response

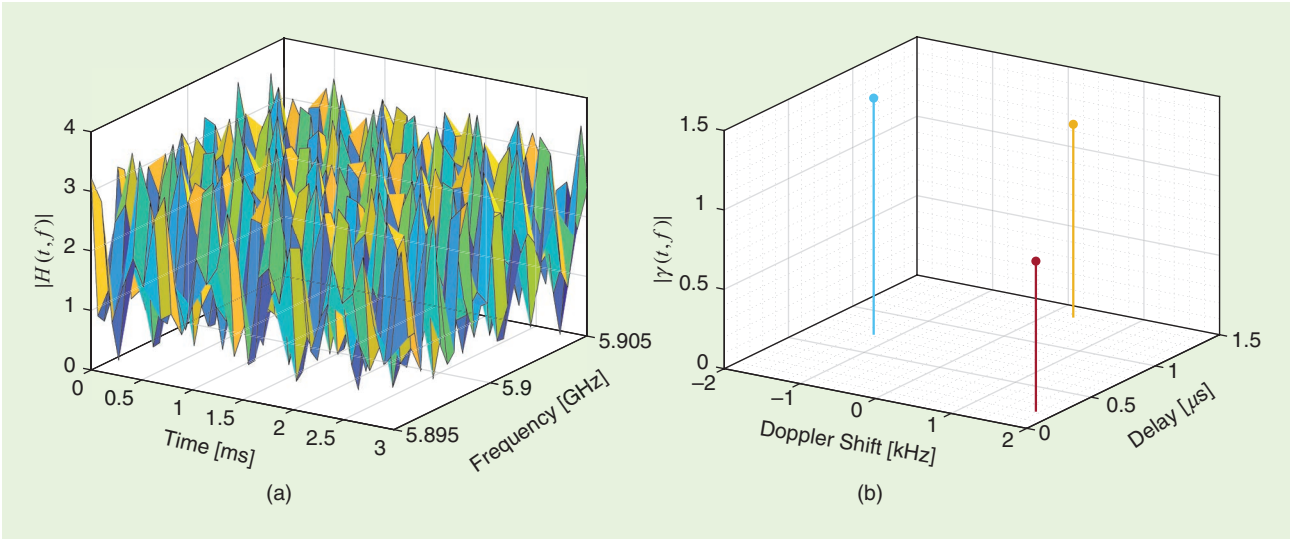

FIGURE 1. The doubly dispersive channel representations with $P = 3$ resolvable paths, with a carrier frequency of 5.9 GHz and signal bandwidth of 10 MHz (following the IEEE 802.11p vehicular environment specifications). The different paths are illustrated by unique colors in Figure 1(b). (a) The TVTF in the time–frequency domain and (b) DVIRF in the delay–Doppler domain.

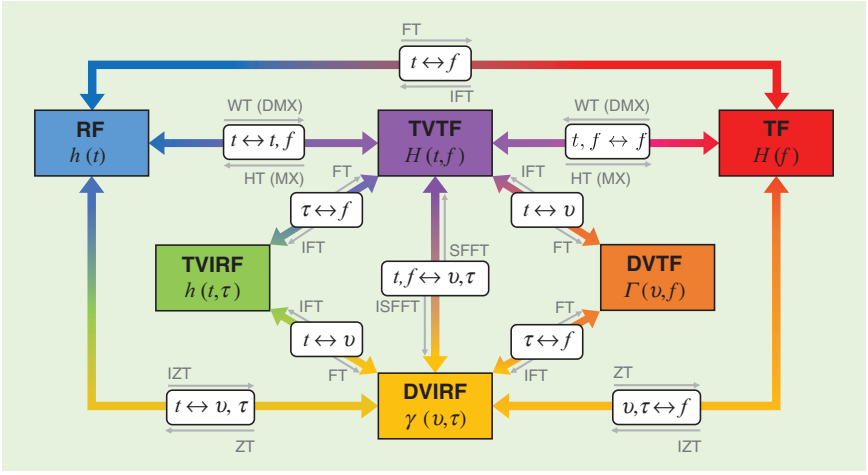

FIGURE 2. The relationship between the different signal domains and inherent transforms. In addition to the illustrated domains, a special case of the time–frequency domain, namely, the chirp domain, also exists, which is omitted in this diagram but elaborated upon in the text. RF: response function; WT: Wigner transform; DMX: de-MX; IFT: inverse FT; HT: Heisenberg transform; DVTF: Doppler-variant transfer function; IZT: inverse Zak transform.

function (DVIRF) in the delay–Doppler domain is obtained by an FT on the TVIRF over the time domain; that is

$$\gamma(\nu,\tau) \triangleq \underset{t\to\nu}{\mathcal{F}}[h(t,\tau)] = \int_{-\infty}^{+\infty} h(t,\tau)\cdot e^{-j2\pi\nu t}\,\mathrm{d}t$$
$$= \sum_{p=1}^{P} h_p \cdot \delta(\nu-\nu_p)\cdot\delta(\tau-\tau_p) \qquad (3)$$

where the time- and frequency-selectivity characteristics are observed in the form of unique impulses in the delay–Doppler plane corresponding to each propagation path, as in Figure 1(b).

It is important to note that the equivalent channel models (1)–(3) are based on a practical approximation of the true doubly dispersive wireless channel, represented in terms of a finite number of significant delay and Doppler frequency taps, which is known to generally work well [4], [14], especially under the underspread environment assumption; i.e., the maximum delay spread $\tau_{\max} - \tau_{\min}$ is smaller than T, the maximum Doppler spread $\nu_{\max} - \nu_{\min}$ is smaller than $1/T$, and $\tau_{\max}\nu_{\max} \ll 1$, where T is the finite signal period, in seconds. (Strictly speaking, a doubly dispersive channel cannot be represented by both finite-delay and Doppler taps, due to the incompatibility of the bandwidth-limited assumption and the temporally limited assumption of the signals. Still, the approximation is well adopted in relevant research and studies [11], [14].)

Following the above, Figure 2 provides a diagram that summarizes the relationships between the among signal domains, including the direction and the integral domain of the necessary linear transforms. Specifically, the rhombus-shaped relationship at the center of the figure illustrates the different domain representations of the doubly dispersive channel as described previously, which also includes the omitted Doppler-variant transfer function (DVTF) in the Doppler frequency domain. (The Doppler frequency domain DVTF is not addressed as often compared to the other three forms, due to its less intuitive relationship with the physical phenomena. However, it is still an equally valid representation of the doubly dispersive channel.)

The Wigner transform and the Heisenberg transform (HT) are generalizations of the MX and de-MX operations of the classical OFDM modulator, which transform a 2D time–frequency-domain signal into the single time and frequency domains. As discussed in the following section, the two transforms can be

respectively implemented using the discrete FT (DFT) and the inverse DFT (IDFT). Furthermore, as can be seen in the figure, there also exist linear transforms that directly describe concatenated FTs and/or inverse FTs (IFTs). Such linear transforms, such as the symplectic finite FT (SFFT) and Zak transform (ZT), are leveraged in the transmitter design of next-generation waveforms, such as the OTFS [7], and are elaborated in the "Signal Models of Next-Generation Waveforms" section.

To wrap up the signal domain fundamentals, let us also address the LCT [12], also known as the *affine FT* (*AFT*), which is a four-parameter transform generalizing many of the popular transforms, such as the FT, Laplace transform (LT), and Fresnel transform.

In particular, the AFT $\underset{t\to u}{\mathcal{L}}[\cdot]$ of a time-domain signal $s(t)$ is described by

$$\underset{t\to u}{\mathcal{L}}[s(t)] \triangleq \begin{cases} \int_{-\infty}^{+\infty} s(t)\cdot\frac{1}{\sqrt{2\pi\,|b|}}\cdot e^{-j\left(\frac{a}{2b}u^2+\frac{1}{b}ut+\frac{d}{2b}t^2\right)}\,\mathrm{d}t, & b\neq 0 \\ s(d\cdot u)\cdot\frac{1}{\sqrt{a}}\cdot e^{-j\frac{cd}{2}u^2} & b=0 \end{cases} \tag{4}$$

where the four AFT parameters (a, b, c, d) are arbitrary complex scalars satisfying $ad-bc=1$. Setting specific parameters reduces the LCT to classical transforms, such as $(0, 1/2\pi, -2\pi, 0)$ for the FT, $(0, j/2\pi, j2\pi, 0)$ for the LT, and $(\cos\theta, (1/2\pi)\sin\theta, -2\pi\sin\theta, \cos\theta)$ to yield the θth order fractional FT.

As will be seen, the available degrees of freedom of the AFT are exploited by another promising waveform, AFDM [11], which allows for the optimization of the AFT parameters based on the channel statistics in order to ensure the orthogonality of the signal in doubly dispersive systems.

Input–output relationship of doubly dispersive channel

The received signal model over the doubly dispersive wireless channel $h(t,\tau)$ in response to a time-domain transmit signal $s(t)$ with bandwidth B is classically described by the linear convolution over the delay domain leveraging the TVIRF representation [4], [14]; namely,

$$\begin{aligned} r(t) &= s(t) * h(t,\tau) + w(t) \\ &\triangleq \int_{-\infty}^{+\infty} s(t-\tau)\left(\sum_{p=1}^{P} h_p\cdot e^{j2\pi\nu_p t}\cdot\delta(\tau-\tau_p)\right)\mathrm{d}\tau + w(t) \end{aligned} \tag{5}$$

where and $r(t)$ and $w(t)$ are respectively the received signal and additive white Gaussian noise (AWGN) in time and * denotes the linear convolution operator.

In turn, assuming that the channel and the AWGN are also band limited by bandwidth B of the transmit signal, sampling (5) at a sampling rate of $f_s \triangleq 1/T_s$ (in hertz) yields the discretized equivalent signal

$$\begin{aligned} r(nT_s) = &\sum_{\ell=0}^{\infty} s(nT_s-\ell T_s)\left(\sum_{p=1}^{P} h_p\cdot e^{j2\pi\nu_p nT_s}\cdot\mathrm{sinc}\left(\ell-\frac{\tau_p}{T_s}\right)\right) \\ &+ w(nT_s) \end{aligned} \tag{6}$$

where $n\in\{0,\ldots,N-1\}$ and $\ell\in\{0,\ldots,N-1\}$ are the discrete time and delay indices, T_s (in seconds) is the sampling period, and $\mathrm{sinc}(x)\triangleq\sin(\pi x)/(\pi x)$ is the normalized sinc function.

The presence of sinc functions resulting from sampling with a finite spectral support can result in interference among the Doppler responses among unique delay taps. However, assuming a wideband communication system as expected in the considered B5G and 6G scenarios, and in aid of oversampling if necessary, the sampling rate f_s will be sufficiently high such that the normalized path delays $\ell_p \triangleq \tau_p f_s = \tau_p/T_s$ can be rounded to the nearest integer with negligible error, i.e., $\ell_p - \lfloor\tau_p/T_s\rceil \approx 0$, or in other words, the sampling resolution T_s is assumed to be sufficiently high such that the normalized path delays ℓ_p are integers [7], [11], [14]. Consequently, the sinc functions are then actually equivalent to unit impulse functions such that (6) can be expressed in terms of the sampled sequences

$$r[n] = \sum_{\ell=0}^{\infty} s[n-\ell]\left(\sum_{p=1}^{P} h_p\cdot e^{j2\pi f_p\frac{n}{N}}\cdot\delta[\ell-\ell_p]\right) + w[n] \tag{7}$$

where $r[n]$, $s[n]$, and $w[n]$ are respectively the sampled sequences of $r(t)$, $s(t)$, and $w(t)$; $f_p \triangleq (N\nu_p/f_s)\in[-(N\nu_{\max}/f_s),(N\nu_{\max}/f_s)]$ is the normalized digital Doppler shift of the pth path; $\ell_p \triangleq (\tau_p/T_s)\in\{0,\ldots,\ell_{\max}\}$ is the normalized integer delay of the pth path; and $\delta[\cdot]$ is the discrete unit impulse function. (Given that the normalized path delays ℓ_p are only integer valued, the sinc functions that take integer input $(\ell-\ell_p)\in\mathbb{N}_0$ yield a value of 1 if $\ell-\ell_p=0$ and a value of 0 otherwise; this is equivalent to the discrete unit impulse function $\delta[\ell-\ell_p]$.)

In addition, in practical multicarrier wireless communications techniques, the transmit sequence in (7) is prepended with a CP to mitigate the effects of time dispersion. The prefix sequence is defined within a CP length of N_{cp} samples, with $N_{\mathrm{cp}}\geq\ell_{\max}$, such that

$$s[n'] = s[N+n']\cdot e^{j2\pi\cdot\phi_{\mathrm{cp}}(n')} \tag{8}$$

where $n'\in\{-1,\ldots,-N_{\mathrm{cp}}\}$ and $\phi_{\mathrm{cp}}(n')$ is a function denoting the multiplicative phase term specific for each waveform, which, for example, is set to zero if the CP does not require a phase offset, as in the OFDM, or a chirp-based phase offset, as in the AFDM, as seen in the following sections.

The CP as described in (8) enables the linear convolutional input–output relation of the TVIRF to be processed as a circular convolutional response. After removing the received signal parts corresponding to the CP, the circular convolutional input–output relationship can be described in matrix form as

$$\begin{aligned} \mathbf{r} \triangleq \mathbf{H}\cdot\mathbf{s} &= \Bigg(\sum_{p=1}^{P} \overbrace{h_p\cdot\mathbf{\Phi}_p\cdot\mathbf{W}^{f_p}\cdot\mathbf{\Pi}^{\ell_p}}^{\triangleq\mathbf{H}_p\in\mathbb{C}^{N\times N}}\Bigg)\cdot\mathbf{s}+\mathbf{w} \\ &= \Bigg(\sum_{p=1}^{P}\mathbf{H}_p\Bigg)\cdot\mathbf{s}+\mathbf{w}\in\mathbb{C}^{N\times 1} \end{aligned} \tag{9}$$

where $\mathbf{r} \in \mathbb{C}^{N\times 1}, \mathbf{s} \in \mathbb{C}^{N\times 1}$, and $\mathbf{w} \in \mathbb{C}^{N\times 1}$ are respectively the vectors representing the received signal, transmit signal, and AWGN; $\mathbf{H} \in \mathbb{C}^{N\times N}$ is the circular convolution effective channel matrix; $\mathbf{\Phi}_p \in \mathbb{C}^{N\times N}$ is the diagonal matrix corresponding to the pth delayed CP phase as given in (10); $\mathbf{W} \in \mathbb{C}^{N\times N}$ is the diagonal matrix containing the Nth roots of unity as given in (11), whose exponentiation by a real number is equivalent to the element-wise exponentiation of the diagonal elements; and $\mathbf{\Pi} \in \mathbb{C}^{N\times N}$ is the forward cyclic shift matrix obtained by left shifting the $N \times N$ identity matrix once, such that right multiplying by $\mathbf{\Pi}^{\ell_p}$ corresponds to a cyclic left shift of a matrix by $\ell_p \in \mathbb{N}_0$ elements. The following is an example of few with $N = 3$,

$$\mathbf{\Pi}^0 \equiv \mathbf{I}_3 = \begin{bmatrix} 1 & 0 & 0 \\ 0 & 1 & 0 \\ 0 & 0 & 1 \end{bmatrix}, \mathbf{\Pi}^1 = \begin{bmatrix} 0 & 0 & 1 \\ 1 & 0 & 0 \\ 0 & 1 & 0 \end{bmatrix}, \text{and } \mathbf{\Pi}^2 = \begin{bmatrix} 0 & 1 & 0 \\ 0 & 0 & 1 \\ 1 & 0 & 0 \end{bmatrix}.$$

As can be seen in (9), the input–output relationship of a doubly dispersive channel is described by a matrix $\mathbf{H}$ consisting of P off diagonals, whose shifted positions are determined by the integer delay of each path. In addition, the complex values along each diagonal contain the channel fading coefficient and the phase offset information of the delayed CP and the Doppler shift of each path. As a consequence of the circulant convolutional channel structure, the different paths are resolvable only in the delay domain and not in the Doppler domain. Therefore, a key design objective of a double-dispersion robust waveform must be the ability to orthogonalize the delays and Doppler shifts of the channel via means of novel domain transforms in the modulation and demodulation of the transmit signal:

$$\mathbf{\Phi}_p \triangleq \text{diag}\,(\overbrace{[e^{-j2\pi\cdot\phi_{\text{cp}}(\ell_p)}, e^{-j2\pi\cdot\phi_{\text{cp}}(\ell_p-1)}, \ldots, e^{-j2\pi\cdot\phi_{\text{cp}}(2)}, e^{-j2\pi\cdot\phi_{\text{cp}}(1)}}^{\ell_p \text{ terms}}, \overbrace{1, 1, \ldots, 1, 1]}^{N-\ell_p \text{ ones}}) \in \mathbb{C}^{N\times N} \tag{10}$$

$$\mathbf{W} \triangleq \text{diag}\,([1, e^{-j2\pi/N}, \ldots, e^{-j2\pi(N-2)/N}, e^{-j2\pi(N-1)/N}]) \in \mathbb{C}^{N\times N}. \tag{11}$$

Multiple-input, multiple-output system model of doubly dispersive channels

Extending the single-input, single-output (SISO) model of the doubly dispersive channel and its received signal model to the multiple-input, multiple-output (MIMO) scenario between a transmitter array equipped with NT antennas and a receiver array equipped with N_R antennas, the received signal $\mathbf{r}_{n_r} \in \mathbb{C}^{N\times 1}$ at the n_rth receive antenna, with $n_r \in \{1, \ldots, N_R\}$, is given by

$$\begin{aligned} \mathbf{r}_{n_r} &\triangleq \sum_{n_t=1}^{N_T} \mathbf{H}_{n_t,n_r}\cdot\mathbf{s}_{n_t} + \mathbf{w}_{n_r} \\ &= \sum_{n_t=1}^{N_T} (\overbrace{\sum_{p=1}^{P} h_{p,n_t,n_r}\cdot\mathbf{\Phi}_p\cdot\mathbf{W}^{f_p}\cdot\mathbf{\Pi}^{\ell_p}}^{\triangleq \mathbf{H}_{n_t,n_r}})\cdot \mathbf{s}_{n_t} + \mathbf{w}_{n_r} \in \mathbb{C}^{N\times 1} \end{aligned} \tag{12}$$

where $\mathbf{H}_{n_t,n_r} \in \mathbb{C}^{N\times N}$ is the convolutional channel between the n_tth transmit antenna and the n_rth receive antenna, with $n_t \in \{1, \ldots, N_T\}$; $\mathbf{s}_{n_t} \in \mathbb{C}^{N\times 1}$ is the transmit signal vector from the n_tth transmit antenna; $h_{p,n_t,n_r} \in \mathbb{C}$ is the complex channel fading coefficient corresponding to the propagation path between the n_tth transmit antenna and the n_rth receive antenna via the pth scatter; and $\mathbf{w}_{n_r} \in \mathbb{C}^{N\times 1}$ is the AWGN vector at the n_rth receive antenna.

Notice that the MIMO received signal model in (12) inherently assumes that the path delays ℓ_p and Doppler shifts f_p are not spatially dependent; i.e., they are identical across all transmit and receive antenna pairs for each propagation path, in accordance to the state-of-the-art (SotA) standardization reports and literature [15]. Therefore, only the complex fading coefficients $h_{p,n_t,n_r} \in \mathbb{C}$ are considered dependent on the specific pth path between the n_tth transmit antenna and the n_rth receive antenna.

However, when beamforming is considered at the MIMO arrays, the effects of spatial filtering [16] introduce angle-dependent antenna gains at the transmitter and/or receiver, which may vary the visibility and, hence, the doubly dispersive channel statistics. To this end, consider an arbitrary transmit beamformer and a receive beamformer applied at the MIMO transmitter and receiver, respectively, where the corresponding transmit beamforming gain at an angle of departure θ^t will be denoted by $f(\theta^t)$ and the receive beamforming gain at an angle-of-arrival θ^r will be denoted by $g(\theta^r)$. Then, the beamformed channel between the n_tth transmit antenna and the n_rth receive antenna is described by

$$\mathbf{H}_{n_t,n_r} = \sum_{p=1}^{P} g(\theta_p^r)\cdot f(\theta_p^t)\cdot h_{p,n_t,n_r}\cdot(\mathbf{\Phi}_p\cdot\mathbf{W}^{f_p}\cdot\mathbf{\Pi}^{\ell_p}) \tag{13}$$

where θ_p^t and θ_p^r are the relative angle of the pth scatterer to the transmitter and the receiver arrays. This model can be generalized to 2D planar arrays incorporating the azimuth and elevation angles of arrival and departure.

Due to the "direction"-dependent gains of the transmit and receive beamformers for each path, it is implied that a given scatterer and its doubly dispersive propagation path is visible to the channel only if it is within the angular range of the major beam. Consequently, the presence of certain scattering paths may be rendered negligible such that for MIMO systems, the doubly dispersive channel statistics, including the delay spread, Doppler spread, and number of significant paths, are beam-space dependent.

Signal models of next-generation waveforms

In this section, we provide the signal models and the transmitter structures of the various waveforms proposed for high performance in the doubly dispersive channel. First, the OFDM waveform is described as a reference, followed by the next-generation waveform candidates, namely, OTFS, and AFDM, in addition to various derivative waveforms that can be related to the latter. (A MATLAB implementation of the doubly dispersive channel model described in this

section, as well as a convenient channel visualization tool used to generate some of the figures, can be found on our online repository.)

OFDM

The well-known OFDM transmitter modulates digital symbols from the frequency domain into a time-domain signal employing an IDFT operation, as demonstrated in Figure 2. Namely, given a vector $\mathbf{x} \in \mathbb{C}^{N\times 1}$ consisting of N complex symbols, the OFDM transmit signal $\mathbf{s}^{\text{OFDM}} \in \mathbb{C}^{N\times 1}$ is given by [17]

$$\mathbf{s}^{\text{OFDM}} = \mathbf{F}_N^{-1}\cdot\mathbf{x} \in \mathbb{C}^{N\times 1} \tag{14}$$

where $\mathbf{F}_N \in \mathbb{C}^{N\times N}$ is the N-point DFT matrix, and hence, $\mathbf{F}_N^{-1} \triangleq \mathbf{F}_N^{\mathsf{H}}$ is the N-point IDFT matrix.

Following the above, the received signal $\mathbf{y}^{\text{OFDM}} \in \mathbb{C}^{N\times 1}$ over the circular convolutional channel described by (9) is demodulated via the forward N-point DFT; i.e.,

$$\mathbf{y}^{\text{OFDM}} = \mathbf{F}_N \overbrace{(\mathbf{H}\cdot\mathbf{s}^{\text{OFDM}} + \mathbf{w})}^{\triangleq\, \mathbf{r}^{\text{OFDM}} \in \mathbb{C}^{N\times 1}} = \overbrace{(\mathbf{F}_N\cdot\mathbf{H}\cdot\mathbf{F}_N^{\mathsf{H}})}^{\triangleq\, \mathbf{G}^{\text{OFDM}} \in \mathbb{C}^{N\times N}}\mathbf{x} + \mathbf{F}_N\cdot\mathbf{w} \in \mathbb{C}^{N\times 1} \tag{15}$$

where, for exposition convenience, we define the OFDM receive signal as $\mathbf{r}^{\text{OFDM}} \in \mathbb{C}^{N\times 1}$ and the effective channel $\mathbf{G}^{\text{OFDM}} \in \mathbb{C}^{N\times N}$ describing the input–output relationship of the baseband OFDM symbols, which can be obtained by combining (9) and (15) to yield

$$\mathbf{G}^{\text{OFDM}} \triangleq \sum_{p=1}^{P} h_p\cdot\mathbf{F}_N(\mathbf{W}^{f_p}\cdot\mathbf{\Pi}^{\ell_p})\mathbf{F}_N^{\mathsf{H}} \tag{16}$$

where the CP phase matrices $\mathbf{\Phi}_p$ existent in (9) have been reduced to identity matrices, as the CP of OFDM signals does not require a phase offset; i.e., $\phi_{\text{cp}}(n) = 0$ in (10).

As shown in Figure 3, the column-wise DFT and row-wise IDFT in the presence of fractional normalized digital Doppler shifts cause the channel diagonals of the convolution matrix to be spread into a decaying band, centered at the original diagonals such that significant interference between each path may arise.

OTFS

In the OTFS modulation scheme, the information symbols are first directly placed in the delay–Doppler domain, instead of the frequency domain as in the OFDM approach, and are then multiplexed into the time signal. Namely, the complex baseband symbols are structured into a 2D grid of size $K \times L$ in the delay–Doppler domain, which is transformed into a time-domain signal via the inverse discrete ZT. Alternatively, as in Figure 2, the equivalent domain transform can be achieved via a two-step process, in which the delay–Doppler signal is first transformed into the time–frequency domain via the ISFFT and then into the continuous-time signal via a pulse-shaping HT. (While mathematically equivalent, in practice, the two-step SFFT-based transform process has been shown to exhibit higher Doppler leakage than the ZT-based counterpart, whose effect decreases with a larger number of subcarriers [18].)

This article will hereafter adopt the more common ISFFT formulation implemented via DFTs/IDFTs. In light of the above, the OTFS modulation process can be described mathematically as

$$\begin{aligned}\mathbf{s}^{\text{OTFS}} &\triangleq \text{vec}\big(\overbrace{\mathbf{P}^{\text{tx}}\mathbf{F}_K^{-1}}^{\text{Pulse-shaping HT}}\cdot\overbrace{(\mathbf{F}_K\mathbf{X}\mathbf{F}_L^{-1})}^{\text{ISFFT}}\big)\\ &= (\mathbf{F}_L^{-1}\otimes\mathbf{P}^{\text{tx}})\cdot\overbrace{\text{vec}(\mathbf{X})}^{\triangleq\,\mathbf{x}} \in \mathbb{C}^{KL\times 1}\end{aligned} \tag{17}$$

where $\mathbf{s}^{\text{OTFS}} \in \mathbb{C}^{KL\times 1}$ is the OTFS transmit signal vector, $\mathbf{X} \in \mathbb{C}^{K\times L}$ is the information symbol matrix consisting of $N \triangleq KL$ complex symbols (without loss of generality, we assume $N \triangleq KL$ to enable direct comparison with 1D modulation schemes, i.e., OFDM), $\mathbf{P}^{\text{tx}} \in \mathbb{C}^{K\times K}$ is the diagonal transmit pulse-shaping filter matrix, $\mathbf{F}_K \in \mathbb{C}^{K\times K}$ and $\mathbf{F}_L \in \mathbb{C}^{L\times L}$ are the K-point and L-point DFT matrices, and $\text{vec}(\cdot)$ and $\otimes$ denote the stacking vectorization and Kronecker product operators, respectively. (The literature commonly assumes a nonideal rectangular pulse shape, which reduces $\mathbf{P}^{\text{tx}}$ to a $K \times K$ identity matrix. However, the specific design of the OTFS pulse-shaping function, in addition to the OTFS time–frequency windowing function [19], is an important design criteria for OTFS that must be addressed to improve the communications and sensing performance.)

The filtered and demodulated signal $\mathbf{y}^{\text{OTFS}}$ after the convolution channel $\mathbf{H}$ in (9) is given by

$$\begin{aligned}\mathbf{y}^{\text{OTFS}} &\triangleq (\mathbf{F}_L\otimes\mathbf{P}^{\text{rx}})\overbrace{(\mathbf{H}\cdot\mathbf{s}^{\text{OTFS}} + \mathbf{w})}^{\triangleq\,\mathbf{r}^{\text{OTFS}} \in \mathbb{C}^{KL\times 1}}\\ &= \mathbf{G}^{\text{OTFS}}\cdot\mathbf{x} + (\mathbf{F}_L\otimes\mathbf{P}^{\text{rx}})\cdot\mathbf{w} \in \mathbb{C}^{KL\times 1}\end{aligned} \tag{18}$$

where $\mathbf{P}^{\text{rx}} \in \mathbb{C}^{K\times K}$ is the diagonal matched filter matrix of $\mathbf{P}^{\text{tx}}$, and the effective OTFS channel $\mathbf{G}^{\text{OTFS}} \in \mathbb{C}^{N\times N}$ in the delay–Doppler domain is given by

$$\mathbf{G}^{\text{OTFS}} \triangleq \sum_{p=1}^{P} h_p\cdot(\mathbf{F}_L\otimes\mathbf{P}^{\text{rx}})(\mathbf{W}^{f_p}\cdot\mathbf{\Pi}^{\ell_p})(\mathbf{F}_L^{\mathsf{H}}\otimes\mathbf{P}^{\text{tx}}) \in \mathbb{C}^{N\times N} \tag{19}$$

which is the convolutional channel matrix $\mathbf{H}$ after a block-wise pulse-shaped DFT and IDFT, and similarly to the OFDM waveform, the CP phase matrices $\mathbf{\Phi}_p$ have been reduced to identity matrices, as the OTFS signal also does not require a phase offset.

It can be observed from (19) that the $KL = N$ elements in each diagonal of the convolutional matrix of (9) are spread into the OTFS effective channel via the block-wise pulse-shaping FTs such that the $KL \times KL$ OTFS channel matrix can be considered a $K \times K$ grid of $L \times L$ submatrices (illustrated as minor grids in Figure 3). In light of the above, the positions of the nonzero channel coefficient elements can be deterministically obtained by the values of both the normalized delay and normalized digital Doppler of each path, respective to the occupied submatrices and the amount of left shift of the diagonals.

If the normalized digital Doppler frequencies are integers, i.e., $f_p \in \mathbb{Z}$ (not the true Doppler frequencies v_p), each path occupies exactly K submatrices out of the $K \times K$ grid in a

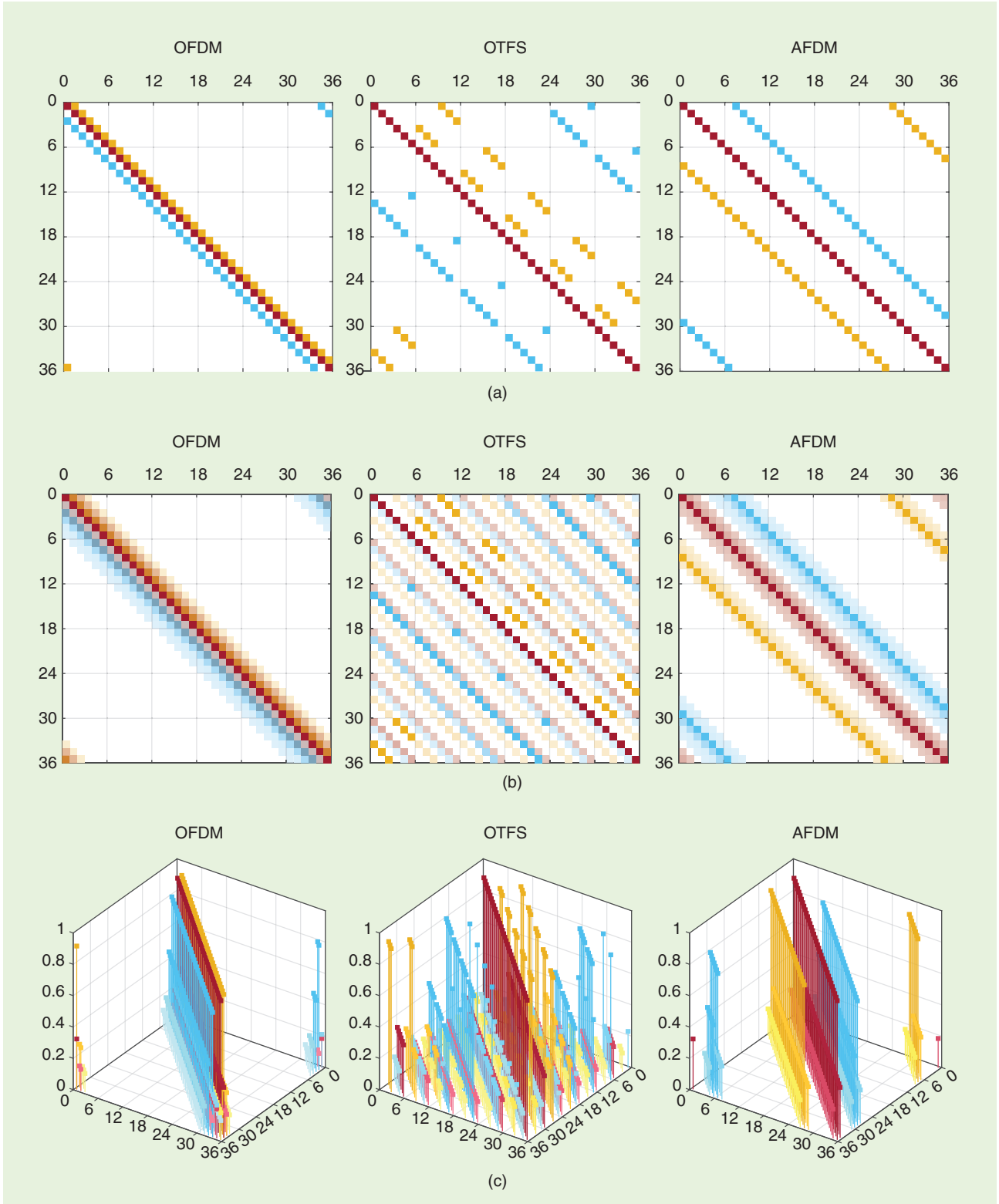

FIGURE 3. Effective channel matrix structures of different waveforms in a doubly dispersive channel with $P = 3$ resolvable paths (each depicted in a different color), with corresponding normalized delays ℓ_p and normalized digital Doppler shifts f_p. The system size parameters are $N = 36$ for the OFDM and AFDM and $K = 6, L = 6$ for the OTFS. The fading colors for the fractional Doppler case correspond to the magnitude of the elements, whereas darker colors correspond to larger powers. Channel components with a magnitude lower than $1/2N$ are considered negligible and not visualized in the figure. (a) Target parameters: $\{\ell_1 = 0, f_1 = 0\}$ (red), $\{\ell_2 = 1, f_2 = -2\}$ (blue), and $\{\ell_3 = 3, f_3 = +1\}$ (yellow). (b) Target parameters: $\{\ell_1 = 0, f_1 = 0.266\}$ (red), $\{\ell_2 = 1, f_2 = -2.365\}$ (blue), and $\{\ell_3 = 3, f_3 = +1.231\}$ (yellow). (c) Target parameters: $\{\ell_1 = 0, f_1 = 0.266\}$ (red), $\{\ell_2 = 1, f_2 = -2.365\}$ (blue), and $\{\ell_3 = 3, f_3 = +1.231\}$ (yellow).

shifted block-diagonal structure, whose amount of right shift is determined by the integer component of the Doppler shift, $f_p^{\text{int}} \triangleq \lfloor f_p \rceil$. For example, a path with $f_p^{\text{int}} = 0$ occupies the K submatrices in the main block-diagonal (a shift of index zero), whereas a path with $f_p^{\text{int}} = 1$ occupies the K submatrices in the block diagonal, which is right shifted by an index of one. On the other hand, for negative Doppler shifts, the block diagonals are left shifted by an index of $\left| f_p^{\text{int}} \right|$, as indicated by path 3 in Figure 3(a).

In turn, each of the K occupied submatrices follows the same structure consisting of exactly L nonzero elements in a shifted diagonal, with a left shift relative to the main diagonal determined by the value of the normalized path delay $\ell_p \in \mathbb{N}$. For example, for a path with delay $\ell_p = 0$, the L nonzero elements are placed in the main diagonal for all K submatrices, whereas a path with $\ell_p = 3$ will have the L nonzero elements in the diagonal left shifted by three indices, for all K submatrices.

It follows that the OTFS waveform can achieve complete orthogonality and resolvability in the delay–Doppler domain, assuming integer values of the normalized delay and normalized digital Doppler shifts and if the channel satisfies the orthogonality condition given by $\ell^{\max} \leq L - 1$ and $f^{\max} \leq \lfloor K/2 \rfloor$, where $\ell^{\max} \triangleq \lceil \tau^{\max}/T_{\text{s}} \rceil$ and $f^{\max} \triangleq \lfloor N\nu^{\max}/f_{\text{s}} \rceil$ are the maximum normalized delay and digital Doppler shift. Note that the orthogonality condition inherently implies that the OTFS waveform will remain orthogonal between unique paths even when the Doppler spread is negligible, i.e., $f^{\max} = 0$, for fixed K and L.

In contrast, in the case of fractional values of the normalized digital Doppler, i.e., $f_p \triangleq f_p^{\text{int}} + f_p^{\text{frac}} \in \mathbb{R}$, where $f_p^{\text{frac}} \in [0.5, +0.5)$, the powers of the channel elements are diffused (or "leaked") across all K^2 submatrices over the main K block-diagonal submatrices of the integer case, resulting in a Doppler domain interference, as presented in Figure 3(b) and (c). The amount of such power leakage is determined by the magnitude of the fractional component of the normalized digital Doppler shift $\left| f_p^{\text{frac}} \right|$ such that larger magnitudes result in more leakage and, hence, more severe interference.

AFDM

In AFDM, a 1D vector of symbols $\mathbf{x} \in \mathbb{C}^{N\times 1}$ is directly multiplexed into a twisted time–frequency chirp domain using the IDAFT [20], as described by

$$\mathbf{s}^{\text{AFDM}} \triangleq \mathbf{A}^{-1}\cdot\mathbf{x} = \overbrace{(\mathbf{\Lambda}_{c_2}\cdot\mathbf{F}_N\cdot\mathbf{\Lambda}_{c_1})^{-1}}^{\text{IDAFT}}\cdot\,\mathbf{x} = (\mathbf{\Lambda}_{c_1}^{\text{H}}\cdot\mathbf{F}_N^{\text{H}}\cdot\mathbf{\Lambda}_{c_2}^{\text{H}})\cdot\mathbf{x} \in \mathbb{C}^{N\times 1} \tag{20}$$

where $\mathbf{A} \triangleq \mathbf{\Lambda}_{c_2}\mathbf{F}_N\mathbf{\Lambda}_{c_1} \in \mathbb{C}^{N\times N}$ is the forward N-point discrete AFT (DAFT) matrix, $\mathbf{\Lambda}_{c_i} \triangleq \text{diag}[e^{-j2\pi c_i(0)^2}, \ldots, e^{-j2\pi c_i(N-1)^2}] \in \mathbb{C}^{N\times N}$ is a diagonal chirp matrix with a central digital frequency of c_i, and the central frequencies c_1 and c_2 of the two diagonal chirps can be optimized to the channel statistics to improve the delay–Doppler orthogonality of the AFDM effective channel. It is shown in [11] that the chirp frequencies c_1 and c_2 are actually correspondent to the four configurable parameters of the AFT formulation in (4).

It follows that the demodulated AFDM signal over the convolution channel in (9) is given by

$$\mathbf{y}^{\text{AFDM}} = \mathbf{A}\cdot\overbrace{(\mathbf{H}\cdot\mathbf{s}^{\text{AFDM}} + \mathbf{w})}^{\triangleq\,\mathbf{r}^{\text{AFDM}}\in\mathbb{C}^{N\times 1}} = \mathbf{G}^{\text{AFDM}}\cdot\,\mathbf{x} + \mathbf{A}\cdot\mathbf{w} \in \mathbb{C}^{N\times 1} \tag{21}$$

with the effective AFDM channel given by

$$\begin{aligned}\mathbf{G}^{\text{AFDM}} \triangleq \sum_{p=1}^{P} h_p\cdot(\mathbf{\Lambda}_{c_2}\cdot\mathbf{F}_N\cdot\mathbf{\Lambda}_{c_1})(\mathbf{\Phi}_p\cdot\mathbf{W}^{f_p}\cdot\mathbf{\Pi}^{\ell_p}) \\ \times(\mathbf{\Lambda}_{c_1}^{\text{H}}\cdot\mathbf{F}_N^{\text{H}}\cdot\mathbf{\Lambda}_{c_2}^{\text{H}}) \in \mathbb{C}^{N\times N}\end{aligned} \tag{22}$$

where the CP phase matrices $\mathbf{\Phi}_p$ require a chirp-cyclic phase offset, described by $\phi_{\text{cp}}(n) = c_1(N^2 + 2Nn)$, which, in the specific case of even N and integer $2Nc_1$, reduces the matrices $\mathbf{\Phi}_p$ back to identity.

The AFDM effective channel can also achieve full orthogonality in the integer normalized delay–Doppler domain when the channel satisfies the orthogonality condition, which is given by

$$2(f^{\max} + \xi)(\ell^{\max} + 1) + \ell^{\max} \leq N \tag{23}$$

where $f^{\max}$ and $\ell^{\max}$ are the maximum normalized digital Doppler shift and delay of the channel and $\xi \in \mathbb{N}_0$ is a free parameter determining the so-called guard width of the AFDM, denoting the number of additional guard elements around the diagonals to anticipate for Doppler-domain interference.

Assuming the orthogonality condition is met, the optimal AFDM chirp frequencies satisfy

$$c_1 = \frac{2(f^{\max} + \xi) + 1}{2N}, \text{ and } c_2 \ll \frac{1}{N} \tag{24}$$

where the flexibility in c_2 enables fine-tuning of the waveform shape, as discussed in the "ISAC Using Next-Generation Waveforms" section.

In light of the above, the position of the shifted diagonal in the AFDM channel can also be described in terms of the integer values of the normalized delay–Doppler indices of each path. Unlike the intricate block-wise structure of the OTFS effective channel, the AFDM effective channel exhibits only a single diagonal per path, which is shifted by a deterministic index dependent on the integer normalized delay ℓ_p and integer normalized digital Doppler shift f_p^{int}. In other words, each diagonal of the convolution channel in (9) is right shifted by an index of exactly $\ell_p\cdot 2(f^{\max} + \xi) + f_p^{\text{int}}$ positions, as in Figure 3(a). On the other hand, in the presence of fractional components of normalized digital Doppler shifts, the diagonals of the AFDM effective channels also exhibit a power leakage around the main diagonal,

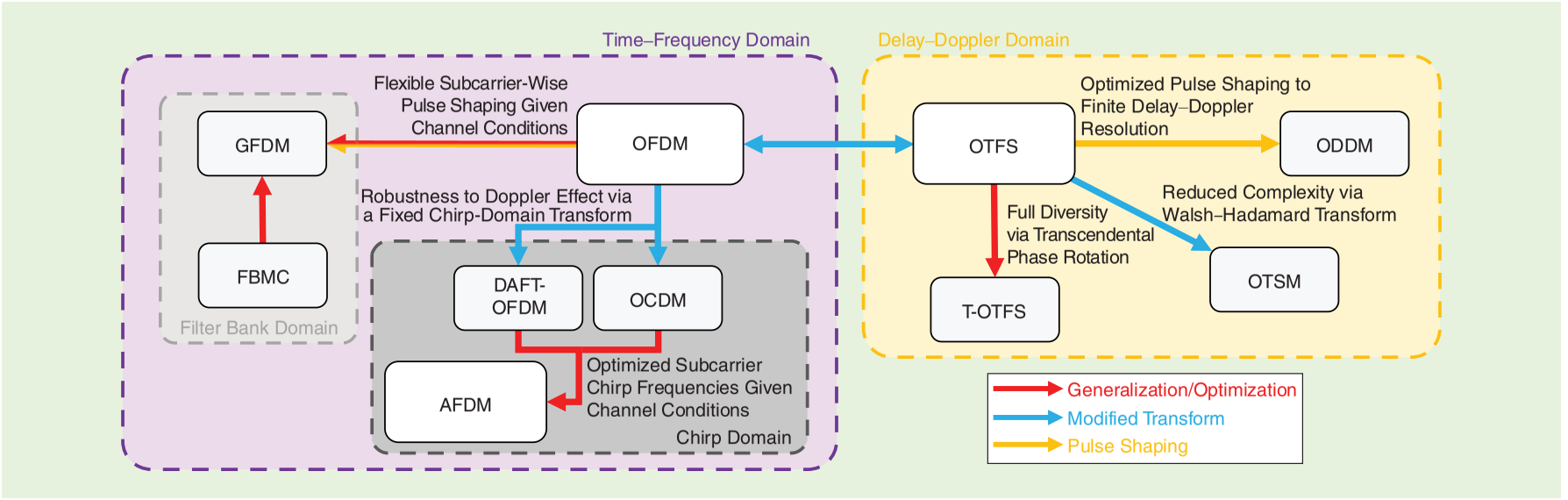

FIGURE 4. Relationships between next-generation waveforms and their signal domains. (a) The time–frequency domain. (b) The delay–Doppler domain. GFDM: generalized frequency-division MX; FBMC: filter bank multicarrier; OCDM: orthogonal chirp division MX; ODDM: orthogonal delay–Doppler division MX; T-OTFS: transcendentally rotated OTFS; OTSM: orthogonal time sequency modulation.

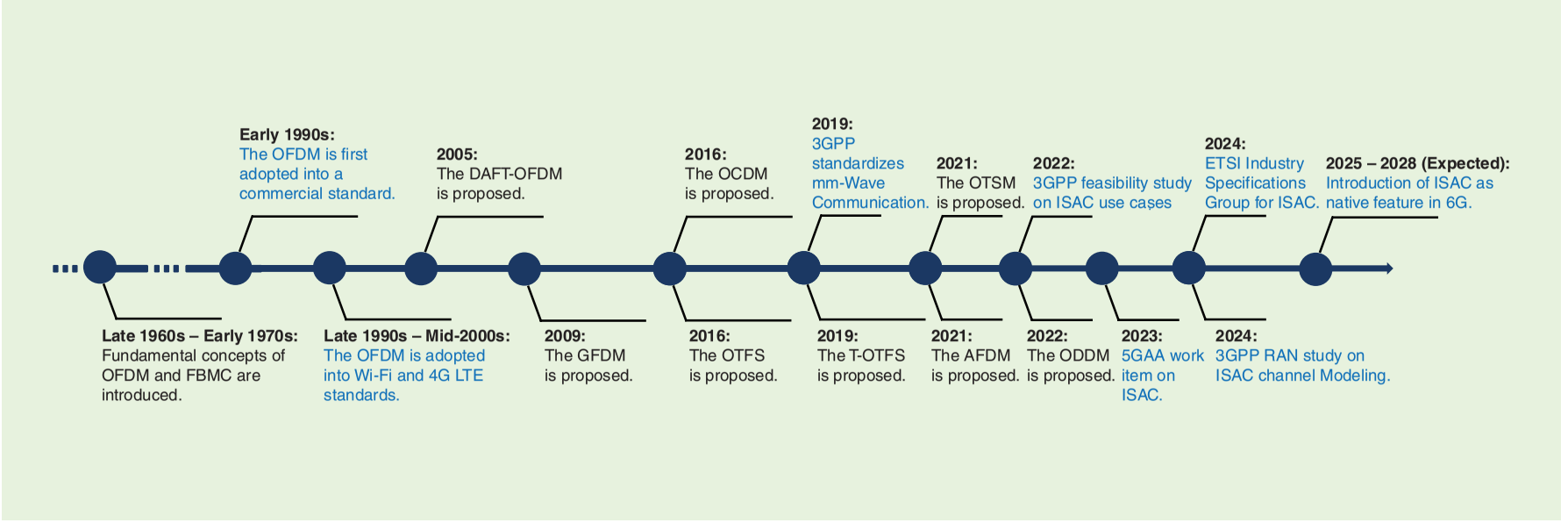

FIGURE 5. A timeline highlighting the invention of various waveforms and key dates in standardization. RAN: radio access network.

resulting in Doppler-domain interference, as can be seen in Figure 3(b) and 3(c).

Related next-generation waveforms

In this section, we briefly discuss various waveforms which, as illustrated in Figure 4 and put into a chronological context in Figure 5, are related to the aforementioned OFDM, OTFS, and AFDM and can also be potential candidates to support ISAC in B5G/6G systems. Due to space limitation, however, the discussion is restricted to a qualitative comparison, addressed in more detail in the "Signal Models of Next-Generation Waveforms" section.

Intermediate chirp-domain waveforms

A few chirp-domain waveforms also exist, which, in commonality with OFDM and AFDM, aim at orthogonalizing delay and Doppler shift indices. Such waveforms, which include orthogonal chirp division MX [10] and DAFT-OFDM [21], can be seen as special cases of AFDM, with nonideal and simplified chirp frequencies c_1 and c_2 [11], naturally exhibiting equal or worse performances depending on the doubly dispersive channel profile.

Enhanced delay–Doppler waveforms

Various methods adopt the novel delay–Doppler signal representation of OTFS and have proposed enhanced delay–Doppler-domain waveforms. Examples are the transcendentally rotated OTFS [22], which maximizes the asymptotic diversity of OTFS via a phase-rotating precoder; orthogonal time sequency modulation [23], which seeks to reduce implementation complexity by leveraging a new type of domain transform; and orthogonal delay–Doppler division MX [24], which improves upon OTFS via an optimized pulse-shaping filter that creates feasible pulses that are orthogonal with respect to the delay–Doppler plane resolution.

Filter bank-based (pulse-shaping) waveforms

Finally, various multicarrier techniques leverage optimized pulse-shaping filter banks, such as the filter bank multicarrier [25] and generalized frequency-division MX (GFDM) [26], which improve the out-of-band emissions, spectral efficiency, ISI, and ICI problems of OFDM via robust adaptation of the subcarriers and modulation pulses with respect to the doubly dispersive channel statistics.

ISAC using next-generation waveforms

In ISAC, wireless "sensing" refers to the ability to harness the rich information about the surrounding environment inherently embedded in radio signals affected by channel conditions. ISAC techniques leveraging a single waveform [this is to distinguish from radar–communication coexistence techniques [6], which "share" the totally available resource (spectrum, antennas, and so on) to allocate and deploy both of the dedicated radar and communications signals] can be classified as either 1) communication-centric designs, which aim to enable the sensing functionality via primary communications waveforms (OFDM, OTFS, AFDM, and so on) by extracting environment/target information from the received signal; 2) radar-centric designs, which aim to enable the communications functionality via primary radar waveforms (pulse, FMCW, and so on) by embedding information to the modulated signal; or 3) dual-functional joint designs, which aim to enable both functionalities via a novelly designed waveform not specific to either of the ISAC functionalities. In this article, we investigate the communication-centric designs in doubly dispersive channels, i.e., enabling the sensing functionality with the aforementioned OFDM, OTFS, and AFDM communications waveforms.

Then, drawing a parallel with well-established radar technologies [27], two distinct types of sensing problems can be identified, namely, 1) the DP, which relates to resolving the number of unique scattering points of interest (targets) from the background clutter, and 2) the EP, which refers to extracting parameters, such as range, velocity, and bearing, associated with the targets. Such sensing scenarios can be classified as monostatic, where the sensing receiver is colocated with the transmitter, or bistatic, where the sensing receiver is spatially remote from the transmitter. The bistatic scenario can be further generalized into a multistatic scenario with multiple distributed transmitters and receivers for several applications and use cases [28]. This scenario is beyond the scope of this article but is an important setting to be addressed in future work, which can enable the full potential of ISAC.

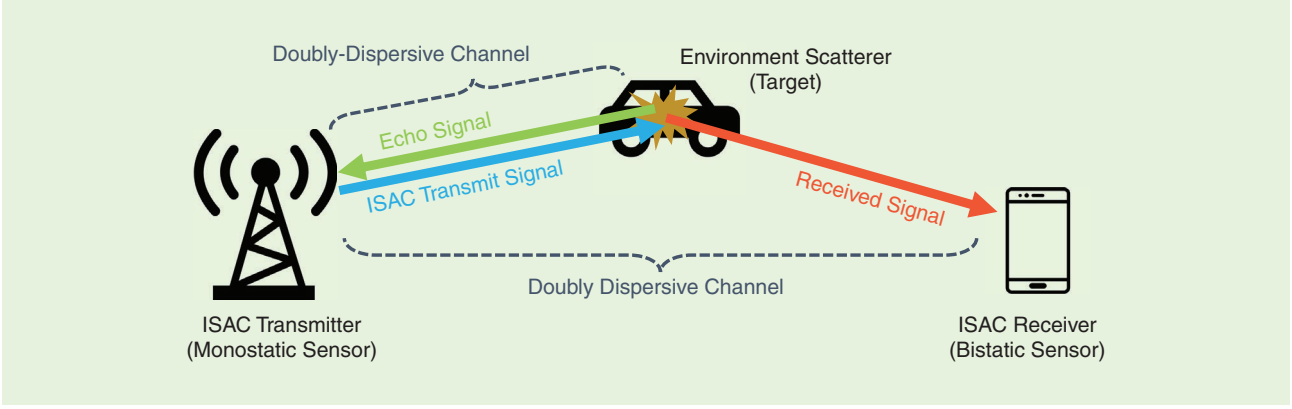

FIGURE 6. Communications and sensing scenarios involved in an ISAC system.

An exemplary ISAC scenario between transmitter and receiver is presented in Figure 6 with a single environment scatterer, where the three subscenarios corresponding to the ISAC functionalities and sensing locations can be observed. Namely, there exist both communications and bistatic sensing subsystems between the ISAC transmitter and the ISAC receiver over the same doubly dispersive channel of the scattering environment and only the monostatic sensing subsystem for the ISAC transmitter.

The radar parameters, namely, the effective range r (in meters) and relative linear velocity v (in meters per second), of the target are directly correspondent to the path delay τ and Doppler shift ν of the target reflected signal:

$$\tau \triangleq \frac{r}{c}, \quad \text{and} \quad \nu \triangleq \frac{2vf_c}{c} \tag{25}$$

where c is the speed of light and f_c is the carrier frequency of the transmitted signal.

For monostatic sensing, the effective range r is twice the range of the target from the colocated transceiver (the round-trip distance), whereas for bistatic scenarios, r is the sum of the transmitter-to-target and receiver-to-target ranges (the total propagation distance). Similarly, for monostatic scenarios, the relative velocity v is in the direction along a straight line between the target and the transceiver, whereas for bistatic scenarios, v is in the direction along the bisecting line between the transmitter-to-target and receiver-to-target paths (the bistatic velocity). In light of the relationship in (25), it is important to notice that the fundamental radar target parameters (range and velocity) are equivalent to the path dispersion parameters (delay and Doppler) of the common doubly dispersive channel, as in Figure 6.

A plethora of OTFS-based ISAC techniques have been proposed to extract the delay and Doppler parameters of the resolvable paths directly from the channel state information.

Solutions to the DPs and EPs can be further classified into three methods based on their approaches: 1) correlation-based methods, in which echo signals are filtered with the known transmit signal in order to yield the radar parameter estimates; 2) direct CSI-based methods, where radar parameters are extracted a posteriori from the known channel matrix; and 3) indirect CSI-based methods, where radar parameters estimation and channel estimation are performed jointly by leveraging the known structure of the doubly dispersive channel of (9). Each of these approaches is discussed further in the sequel.

In the scope of this article, we address only the radar parameter estimation of the SISO model, as the MIMO extension can be trivially derived by leveraging the models in (12) and (13) with the corresponding MIMO radar processing techniques [16]. This enables the estimation of the bearing, i.e., the angular direction of the scatterer targets, and in the case of 2D planar arrays, the azimuth and elevation angles of the target in 3D space.

Correlation-based methods

Classical radar systems based on chirps and impulsive waveforms [27] are typical examples of the correlation-based method, as the received echo signals are processed by a correlation (matched filter) with a known probing signal to directly yield the target parameters. Radar waveforms are, however, optimized to exhibit correlation properties that can achieve high resolution in the delay and Doppler domains, which is generally not possible to do with communication waveforms without sacrificing communication objectives (e.g., rate, efficiency, latency, and so on).

The fundamental resolution of the correlation-based method can be analyzed through the well-known 2D ambiguity function of a waveform in the delay–Doppler domain (in the case for MIMO, the dimension of the ambiguity function is extended to include the angular domain), which is given by

$$A(\tau,\nu) \triangleq \int_{-\infty}^{+\infty} s(t)\cdot s^*(t-\tau)\cdot e^{j2\pi\nu t}\,\mathrm{d}t \tag{26}$$

where $A(\tau,\nu)$ is the 2D ambiguity function parametrized by the delay and Doppler shift values, $s(t)$ is the transmit signal, and $(\cdot)^*$ denotes the complex conjugation operation.

By inspecting the ambiguity function behaviors of the OFDM, OTFS, and AFDM waveforms [29], the different delay–Doppler resolution and beam lobe behaviors of the waveforms can be observed. Namely, it is found that that OFDM shows high resolution in the delay domain but not in the Doppler domain, whereas OTFS and AFDM show moderate resolution in both domains simultaneously, with AFDM exhibiting an adjustable main lobe width with a tradeoff in the two domains by leveraging the chirp frequency parameters c_1 and c_2. Therefore, naturally, correlation-based estimators of low complexity, employing OFDM, OTFS, and AFDM [29], [30], [31], have been proposed but were found to still be fundamentally dependent on the resolution of the ambiguity function, promoting subsequent development of parameter estimation methods based on the higher resolution of the inherent delay–Doppler modulation grid.

Furthermore, it is important to notice that correlation-based methods inherently require the full knowledge of the transmit signal. Therefore, in consideration of the ISAC regime, its application is feasible only for monostatic sensing scenarios in which the transmit signal is fully known or for bistatic scenarios by leveraging transmission frames with a known sequence, such as a pilot or preamble.

Direct CSI-based methods

These methods operate under the assumption that channel estimation (CSI acquisition) has already been performed at the ISAC receiver such that the effective channel matrix is available numerically, i.e., as complex taps of the channel

matrix, and aim to extract radar parameters a posteriori by exploiting the deterministic structure of the doubly dispersive channel, as described in the "Signal Models of Next-Generation Waveforms" section. Several sensing algorithms based on this approach have been proposed. Assuming that CSI is obtained in the time–frequency domain as per (2), the resulting EP on τ_p and ν_p is referred to as a *multidimensional harmonic retrieval problem*, to which many well-known superresolution solutions exist, such as multiple signal classification and estimation of signal parameters via rotational invariance techniques, in addition to enhanced tensor-based algorithms in the case of MIMO scenarios with increased dimensionality, as discussed in [6]. The approach is known to achieve high resolution and accuracy but typically requires a large number of continuously obtained observation samples, which, together with the fundamental dependence on the channel estimation performance, constitute a prominent challenge of such methods since channel estimation errors may propagate to the radar parameter estimates.

Setting these issues aside, with a sufficiently large number of observations and appropriate filtering, the effective channel matrices of the waveforms as given in (16), (19), and (22) may be obtained via compressive sensing and other matrix reconstruction algorithms. In such cases, the delay–Doppler orthogonality of the OTFS and AFDM effective channels, in addition to the injective mapping between each integer delay–Doppler pair and the position of the shifted-diagonal, as discussed in the "Signal Models of Next-Generation Waveforms" section, enable efficient extraction of the target parameters from the channel matrix element positions. However, in the presence of fractional Doppler shifts, the resulting interference in the Doppler domain in Figure 3(b) can significantly deteriorate such "position-based" methods in terms of Doppler resolution.

An alternative strategy to design ISAC-friendly and mobility-robust waveforms is to employ chirp-based multicarrier approaches.

Since the direct CSI-based method inherently assumes the full knowledge of the effective channel matrix, which requires a dedicated channel estimation step involving a known transmit signal, this is also possible only for monostatic sensing scenarios or for bistatic scenarios with a dedicated pilot.

Indirect CSI-based methods (integrated channel estimation)

In cases where the channel matrix is not available but its structure is known, an EP can be formulated to jointly estimate the channel inherently incorporating the radar parameters, yielding an integrated channel and target parameter estimation. Such scenarios are expected at ISAC receivers where the information of the transmit signal is available but channel estimation has not been performed or at bistatic ISAC receivers with unknown components of the transmit signal (i.e., information symbols).

When the transmit signal is fully known, the following minimization problem can be solved:

$$\underset{\tau_p,\nu_p,h_p\forall p}{\operatorname{argmin}} \mathcal{L}(\mathbf{y}-\tilde{\mathbf{G}}(\tau_p,\nu_p,h_p;\forall p)\cdot\mathbf{x}) \tag{27}$$

where $\mathbf{y}\triangleq\mathbf{G}\mathbf{s}+\mathbf{w}\in\mathbb{C}^{N\times 1}$ is the demodulated received signal—where $\mathbf{G}$ is the effective channel corresponding to the specific waveform, $\tilde{\mathbf{G}}(\tau_p,\nu_p,h_p;\forall p)\in\mathbb{C}^{N\times N}$ is the estimated effective channel parametrized by the three P parameters τ_p,ν_p,h_p for $p\in\{1,\ldots,P\}$, and $\mathbf{s}\in\mathbb{C}^{N\times 1}$ is the transmit symbol vector—and $\mathcal{L}(\cdot)$ is an arbitrary objective function, i.e., the L_2 norm.

In the doubly dispersive case, the parametrized channel $\tilde{\mathbf{H}}$ is given by (9) or preprocessed via leveraging the effective channel models of specific waveforms described, e.g., by (16), (19), or (22), for OFDM, OTFS, and AFDM, respectively.

On the other hand, when parts of the transmit signal are also unknown, a bilinear estimation is required in the form of a joint channel and data estimation problem on the system, described by

$$\mathbf{y}=\tilde{\mathbf{G}}(\tau_p,\nu_p,h_p;\forall p)\cdot\tilde{\mathbf{x}}\in\mathbb{C}^{N\times 1} \tag{28}$$

where $\mathbf{y}\in\mathbb{C}^{N\times 1}$ is the demodulated received signal, $\tilde{\mathbf{G}}(\tau_p,\nu_p,h_p;\forall p)\in\mathbb{C}^{N\times N}$ is the estimated effective channel matrix parametrized by the three P parameters, and $\tilde{\mathbf{x}}\in\mathbb{C}^{N\times N}$ is the estimated transmit symbol vector composed of known pilot symbols and unknown information symbols.

The joint estimation of the unknown data symbols and the unknown channel parametrized by the three P radar parameters is therefore an inherently equivalent problem to the joint target detection and data estimation, which can be solved via a plethora of methods, as elaborated in the following section.

Estimation methods of CSI-based methods

There are largely two approaches to the underlying three-P-parameter EP present in CSI matrix-based sensing methods in the "Direct CSI-Based Methods" and "Indirect CSI-Based Methods (Integrated Channel Estimation)" sections: 1) on-grid search-based methods, which yield values corresponding to the resolution of the discretized parameter grid, and 2) off-grid methods, which directly yield a continuous estimate of the parameters.

On-grid methods [32], [33] assume the domain of the path delay and Doppler shift to be discrete on a given grid resolution, typically of the discretely sampled signal and channel, and solve the optimization problem via maximum likelihood (ML), i.e., a search over the discrete parameter solution space. Typically, the parameter grid is initially limited to the sampling frequency, which consists of the integer values of the normalized delay and normalized digital Doppler frequency. However, a common approach is to first obtain the on-grid "coarse" integer estimates of the parameters, then perform an iterative search around the estimate with a virtually subdivided grid. Such subdivisions can be refined to arbitrarily high resolutions

but trivially require higher complexity, as the estimation still requires an optimization over the discrete subdivided grid.

On the other hand, off-grid methods directly yield a continuous estimate of the radar parameters by leveraging a variety of techniques, including message passing, Bayesian learning, convex optimization, harmonic retrieval, and so on [34], [35]. Such methods are not restricted by the resolution of the sampling frequency or a discrete grid and capable of directly estimating the fractional components of the parameters, but as they are not ML, they may be more prone to the error caused by the noise and interference and may exhibit an algorithmic resolution limit (i.e., error floor).

Novel delay–Doppler orthogonal designs of OTFS and AFDM benefit the signal processing for both communication and sensing functionalities, advocating the integration of the two.

Furthermore, the fractional components of the Doppler shift cause spectral leakage around the main peaks of the effective channel, as described in the "Signal Models of Next-Generation Waveforms" section and illustrated in Figure 3(c), which makes the effective channel less sparse and subject to interference among the channel components of different paths. Depending on the specific algorithm utilized for parameter estimation, such suboptimal structures of the effective channel without proper alleviation techniques can deteriorate the sensing performance.

KPI-centered comparative analysis

In view of all the above, we finally offer a qualitative comparison of OFDM, OTFS, and AFDM, respectively representing the classic, SotA, and most recent alternative, ISAC-friendly waveforms for B5G/6G systems. To this end, we consider various relevant KPIs for communication and sensing functions, both in terms of features and implementation aspects. The GFDM and FMCW waveforms are also included for comparison, communications, and radar sensing performances, respectively.

The result is given in Table 1, and while it is not possible to elaborate on all comparison points, due to space limitations, we briefly elaborate on a few most important of the selected KPIs. In particular, perhaps the most important communications KPI in doubly dispersive channels is the Doppler shift robustness, i.e., the compatibility to high-mobility and EHF conditions, which is attained only by the OTFS and AFDM waveforms, due to the inherent delay–Doppler-domain orthogonality. In this aspect, it is noteworthy that OTFS achieves full diversity only in finite signal-to-noise ratio regimes converging to first-order asymptotic diversity [22], while AFDM provides guaranteed full diversity generally [11] and is also known to be the only Doppler-robust

Table 1. A comparison of various waveforms and their ISAC KPIs, with qualitative measures: high, medium, and low.

			Waveform			
		KPI	**OFDM**	**OTFS**	**AFDM**	**GFDM**
Communications	Performance	Waveform domain	Time–frequency	Delay–Doppler	Chirp	Filter bank
		Delay robustness	High	High	High	High
		Doppler robustness	Low	High	High	Medium
		Peak-to-average power ratio	High	Low	High	Medium
		Diversity in TV channels	Low	Medium	High	Medium
		Frame guard (CP) overhead	High	Low	Medium	Medium
		Pilot guard overhead	Medium	High	Low	Medium
	Implementation	Modulation complexity	Low	High	Medium	High
		OFDM compatibility	High	High	High	High
		Power amplifier strain	High	Low	High	Medium
		MIMO scalability	High	Medium	High	Medium
		EHF feasibility	Low	High	High	Medium
		Full-duplex potential	Low	Medium	High	Medium
		KPI	**OFDM**	**OTFS**	**AFDM**	**FMCW**
Target sensing	Performance	Delay ambiguity	Low	Medium	Variable	Low
		Doppler ambiguity	High	Medium	Variable	Low
		Peak-to-sidelobe ratio	Medium	Low	Variable	Low
		Maximum unambiguous range	Medium	Medium	Medium	High
		Maximum unambiguous velocity	Medium	Medium	Medium	High
	Implementation	Implementation cost	Low	Medium	Medium	Low
		Engineering complexity	Low	Medium	Medium	Low
		MIMO array extendibility	High	Medium	High	High
		ISAC feasibility	Medium	High	High	Medium

The color of each cell corresponds to the relative performance measure, ranging from green, denoting an attractive performance, to yellow, to red, denoting less performant.

waveform to also achieve full diversity in MIMO scenarios. On the other hand, due to their fundamental roots in OFDM, both AFDM and GFDM also suffer from a higher peak-to-average power ratio (PAPR), whereas OTFS enjoys a low PAPR due to the DFT-based spreading of the symbol powers in the time–frequency domain. This advantage is closely linked to implementation cost and hardware stability, especially in relation to the power amplifier and radio-frequency component efficiency, which becomes more prominent in the massive MIMO scenarios.

Another important point to consider is the computational complexity, which is linked to various signal processing procedures, such as modulation and channel estimation. In this regard, while both OTFS and AFDM can be interpreted as modified precoding schemes for OFDM transmitters such that core OFDM modulators can be reused, the 1D AFDM modulator exhibits a higher efficiency than the 2D OTFS modulator. This reduced dimension of the waveform also shows a similar advantage for channel estimation, in terms of both computational complexity and the required piloting overhead.

In terms of target sensing performance, OTFS and AFDM exhibit a significant improvement in the Doppler-domain ambiguity over OFDM, but such methods are restricted, as they are not optimized for correlation as with FMCW waveforms. Therefore, superresolution methods and on-grid estimation methods on the discrete delay–Doppler domain of the waveforms are leveraged, which can achieve extremely high resolutions compared to those of FMCW, often used in automotive radar, given sufficient parameterization, such as the carrier frequency and symbol period.

The above-described properties in both communications and sensing performances must be satisfied and be coherent in order for a waveform to be considered a strong candidate for ISAC in B5G/6G. Clearly, as observed from the color scaling of Table 1, OTFS and AFDM are the most promising candidates satisfying most of the ISAC criteria, with some tradeoffs between the two waveforms in terms of complexity, power, and spectral efficiency, which is to be further addressed in a future work.

Future works

It can be seen that while OTFS and AFDM are the most promising candidates to enable high-performance ISAC for next-generation wireless networks, there are still many important topics to be addressed in order to enable the incorporation of such techniques into future standards. Indeed, any given row of Table 1, such as the PAPR of AFDM or the CSI estimation complexity of OTFS, can be a subject of optimization and development. The authors hope that this article helps the ISAC research community with fundamental insights, techniques, and future directions to promote the development of high-performance ISAC in doubly dispersive environments for next-generation wireless networks. Furthermore, in light of the consolidated fundamentals and the identification of potentials and challenges of the doubly dispersive environment and the promising waveforms, it is also important to investigate the implications toward the consequent practical implementations and design.

Acknowledgment

The work of Yong Liang Guan is supported under the RIE2020 Industry Alignment Fund-Industry Collaboration Projects (IAF-ICP) Funding Initiative, as well as cash and in-kind contribution from the industry partner(s).

Authors

Hyeon Seok Rou (hrou@constructor.university) received his B.Sc. degree in 2021 from Jacobs University Bremen, Germany. He is a Ph.D. candidate in the School of Computer Science and Engineering, Constructor University, 28759 Bremen, Germany. His research interests include integrated sensing and communications, B5G/V2X communications systems, doubly dispersive channels, Bayesian inference, and massive index modulation. He is a Graduate Student Member of IEEE.

Giuseppe Thadeu Freitas de Abreu (gabreu@constructor.university) received his D.Eng. degree in 2004 from Yokohama National University, Japan. He is a professor at the School of Computer Science and Engineering, Constructor University, 28759 Bremen, Germany. He is currently the editor of *IEEE Signal Processing Letters* and *IEEE Communications Letters*. His research interests include communications theory, estimation theory, statistical modeling, wireless localization, cognitive radio, wireless security, MIMO systems, ultrawideband and millimeter wave communications, full-duplex and cognitive radio, compressive sensing, energy harvesting networks, random networks, and connected vehicles networks. He is a Senior Member of IEEE.

Junil Choi (junil@kaist.ac.kr) received his Ph.D. degree in 2015 from Purdue University. He is a tenured associate professor in the School of Electrical Engineering, at the Korea Advanced Institute of Science and Technology, 34141 Daejeon, South Korea. He is the area editor of the IEEE Open Journal of the Communications Society and the associate editor of *IEEE Transactions on Wireless Communications* and *IEEE Transactions on Communications*. His research interests include design and analysis of massive MIMO, mmWave communication systems, distributed reception, vehicular communication systems. He is a Senior Member of IEEE.

David González G. (david.gonzalez.g@ieee.org) received his Ph.D. degree in 2013 from the Universitat Politècnica de Catalunya, Spain. He is a wireless communications researcher at Continental AG, 60488 Frankfurt am Main, Germany and a delegate in 3GPP RAN1, 5GAA, and ETSI ISG ISAC. His research interests include vehicular communications (V2X), integrated sensing and communications (ISAC), and automotive applications for 5G-Advanced and 6G. He is a Senior Member of IEEE.

Marios Kountouris (marios.kountouris@eurecom.fr) received his Ph.D. degree in 2008 from Télécom ParisTech, France. He is a professor in the Communication Systems Department, EURECOM, France. He is the editor of *IEEE*

Transactions on Wireless Communications, Transactions on Signal Processing, and *IEEE Wireless Communication Letters*. He is an AAIA Fellow and a professional engineer of the Technical Chamber of Greece. His research interests include communication theory, wireless networks, deep learning, and quantum information science. He is a Fellow of IEEE.

Yong Liang Guan (eylguan@ntu.edu.sg) received his Ph.D. degree in 1997 from Imperial College London, U.K. He is a professor in the School of Electrical and Electronic Engineering, Nanyang Technological University (NTU), 639798 Singapore. He is the associate vice president of Nanyang Technological University, Singapore, a Distinguished Lecturer in the IEEE Vehicular Technology Society, and editor of *IEEE Transactions on Vehicular Technology*. His research interests include coding and signal processing for communication systems and data storage systems. He is a Senior Member of IEEE.

Osvaldo Gonsa (osvaldo.gonsa@continental-corporation.com) received his Ph.D. degree in 1999 from Yokohama National University, Japan, and his M.B.A. in 2012 from Kempten School of Business, Germany. He is the head of Wireless Communications Technologies Growth Field, Continental AG, 60488 Frankfurt am Main, Germany. He serves on the GSMA Advisory Board for Automotives, and he is the main representative of Continental AG at the 5GAA association. His research interests include 5G-Advanced/6G research and standardization.

References

[1] T. S. Rappaport et al., "Wireless communications and applications above 100 GHz: Opportunities and challenges for 6G and beyond," *IEEE Access*, vol. 7, pp. 78,729–78,757, 2019, doi: 10.1109/ACCESS.2019.2921522.

[2] N.-S. Vo, T. Q. Duong, and Z. Sheng, "The key trends in B5G technologies, services and applications," *Mobile Netw. Appl.*, vol. 27, no. 4, pp. 1716–1718, 2022, doi: 10.1007/s11036-022-01999-3.

[3] Y. Zhong et al., "Empowering the V2X network by integrated sensing and communications: Background, design, advances, and opportunities," *IEEE Netw.*, vol. 36, no. 4, pp. 54–60, Jul./Aug. 2022, doi: 10.1109/MNET.001.2100688.

[4] D. Bliss and S. Govindasamy, *Dispersive and Doubly-Dispersive Channels*. Cambridge, U.K.: Cambridge Univ. Press, 2013.

[5] T. Wang, J. Proakis, E. Masry, and J. Zeidler, "Performance degradation of OFDM systems due to doppler spreading," *IEEE Trans. Wireless Commun.*, vol. 5, no. 6, pp. 1422–1432, Jun. 2006, doi: 10.1109/TWC.2006.1638663.

[6] J. A. Zhang et al., "Enabling joint communication and radar sensing in mobile networks—A survey," *IEEE Commun. Surv. Tut.*, vol. 24, no. 1, pp. 306–345, Firstquarter 2022, doi: 10.1109/COMST.2021.3122519.

[7] Z. Wei et al., "Orthogonal time-frequency space modulation: A promising next-generation waveform," *IEEE Wireless Commun.*, vol. 28, no. 4, pp. 136–144, Aug. 2021, doi: 10.1109/MWC.001.2000408.

[8] W. Anwar et al., "Performance analysis of various waveforms and coding schemes in V2X communication scenarios," in *Proc. IEEE Wireless Commun. Netw. Conf. (WCNC)*, Seoul, Korea (South), 2020, pp. 1–8, doi: 10.1109/WCNC45663.2020.9120732.

[9] L. Gaudio, M. Kobayashi, G. Caire, and G. Colavolpe, "On the effectiveness of OTFS for joint radar parameter estimation and communication," *IEEE Trans. Wireless Commun.*, vol. 19, no. 9, pp. 5951–5965, Sep. 2020, doi: 10.1109/TWC.2020.2998583.

[10] X. Ouyang and J. Zhao, "Orthogonal chirp division multiplexing," *IEEE Trans. Commun.*, vol. 64, no. 9, pp. 3946–3957, Sep. 2016, doi: 10.1109/TCOMM.2016.2594792.

[11] A. Bemani, N. Ksairi, and M. Kountouris, "Affine frequency division multiplexing for next generation wireless communications," *IEEE Trans. Wireless Commun.*, vol. 22, no. 11, pp. 8214–8229, Nov. 2023, doi: 10.1109/TWC.2023.3260906.

[12] J. J. Healy, M. A. Kutay, H. M. Ozaktas, and J. T. Sheridan, *Linear Canonical Transforms: Theory and Applications*, vol. 198. New York, NY, USA: Springer-Verlag, 2015.

[13] Nokia, "RP-234069: Study on channel modelling for integrated sensing and communication (ISAC) for NR," Nokia Shanghai Bell, Shanghai, China. Tech. Rep., RAN Meeting #102, Dec 2023.

[14] Y. Hong, T. Thaj, and E. Viterbo, *Delay-Doppler Communications: Principles and Applications*. New York, NY, USA: Academic, 2022.

[15] ETSI, "ETSI TR 125 996 V17.0.0 - Universal mobile telecommunications system (UMTS); spatial channel model for multiple input multiple output (MIMO) simulations (3GPP TR 25.996 Version 17.0.0 Release 17)," Tech. Rep., 2022. [Online]. Available: https://cdn.standards.iteh.ai/samples/71158/eef2c-791ca2e4657aaaf3666b336f13c/ETSI-TR-125-996-V18-0-0-2024-05-.pdf

[16] J. Li and P. Stoica, *MIMO Radar Signal Processing*. Hoboken, NJ, USA: Wiley, 2008.

[17] R. Prasad, *OFDM for Wireless Communications Systems*. Norwood, MA, USA: Artech House, 2004.

[18] V. S. Bhat, G. Harshavardhan, and A. Chockalingam, "Input-output relation and performance of RIS-aided OTFS with fractional delay-doppler," *IEEE Commun. Lett.*, vol. 27, no. 1, pp. 337–341, Jan. 2023, doi: 10.1109/LCOMM.2022.3214678.

[19] Z. Wei, W. Yuan, S. Li, J. Yuan, and D. W. K. Ng, "Transmitter and receiver window designs for orthogonal time-frequency space modulation," *IEEE Trans. Commun.*, vol. 69, no. 4, pp. 2207–2223, Apr. 2021, doi: 10.1109/TCOMM.2021.3051386.

[20] S.-C. Pei and J.-J. Ding, "Closed-form discrete fractional and affine Fourier transforms," *IEEE Trans. Signal Process.*, vol. 48, no. 5, pp. 1338–1353, May 2000, doi: 10.1109/78.839981.

[21] T. Erseghe, N. Laurenti, and V. Cellini, "A multicarrier architecture based upon the affine Fourier transform," *IEEE Trans. Commun.*, vol. 53, no. 5, pp. 853–862, May 2005, doi: 10.1109/TCOMM.2005.847162.

[22] G. D. Surabhi, R. M. Augustine, and A. Chockalingam, "On the diversity of uncoded OTFS modulation in doubly-dispersive channels," *IEEE Trans. Wireless Commun.*, vol. 18, no. 6, pp. 3049–3063, Jun. 2019, doi: 10.1109/TWC.2019.2909205.

[23] T. Thaj, E. Viterbo, and Y. Hong, "Orthogonal time sequency multiplexing modulation: Analysis and low-complexity receiver design," *IEEE Trans. Wireless Commun.*, vol. 20, no. 12, pp. 7842–7855, Dec. 2021, doi: 10.1109/TWC.2021.3088479.

[24] H. Lin and J. Yuan, "Orthogonal delay-doppler division multiplexing modulation," *IEEE Trans. Wireless Commun.*, vol. 21, no. 12, pp. 11,024–11,037, Dec. 2022, doi: 10.1109/TWC.2022.3188776.

[25] B. Farhang-Boroujeny, "OFDM versus filter bank multicarrier," *IEEE Signal Process. Mag.*, vol. 28, no. 3, pp. 92–112, May 2011, doi: 10.1109/MSP.2011.940267.

[26] N. Michailow et al., "Generalized frequency division multiplexing for 5th generation cellular networks," *IEEE Trans. Commun.*, vol. 62, no. 9, pp. 3045–3061, Sep. 2014, doi: 10.1109/TCOMM.2014.2345566.

[27] M. A. Richards, *Fundamentals of Radar Signal Processing*. New York, NY, USA: McGraw-Hill, 2005.

[28] H. S. Rou et al., "Integrated sensing and communications for 3D object imaging via bilinear inference," *IEEE Trans. Wireless Commun.*, to be published, doi: 10.1109/TWC.2024.3352975.

[29] J. Zhu et al., "A low-complexity radar system based on affine frequency division multiplexing modulation," 2023, *arXiv:2312.11125*.

[30] P. Kumari, J. Choi, N. González-Prelcic, and R. W. Heath, "IEEE 802.11ad-based radar: An approach to joint vehicular communication-radar system," *IEEE Trans. Veh. Technol.*, vol. 67, no. 4, pp. 3012–3027, Apr. 2018, doi: 10.1109/TVT.2017.2774762.

[31] P. Raviteja, K. T. Phan, Y. Hong, and E. Viterbo, "Orthogonal time frequency space (OTFS) modulation based radar system," in *Proc. IEEE Radar Conf. (RadarConf)*, Boston, MA, USA, 2019, pp. 1–6, doi: 10.1109/RADAR.2019.8835764.

[32] M. F. Keskin, H. Wymeersch, and A. Alvarado, "Radar sensing with OTFS: Embracing ISI and ICI to surpass the ambiguity barrier," in *Proc. IEEE Int. Conf. Commun. Workshops (ICC Workshops)*, Montreal, QC, Canada, 2021, pp. 1–6, doi: 10.1109/ICCWorkshops50388.2021.9473534.

[33] K. R. R. Ranasinghe, H. S. Rou, and G. T. F. de Abreu, "Fast and efficient sequential radar parameter estimation in MIMO-OTFS systems," in *Proc. IEEE Int. Conf. Acoust. Speech Signal Process. (ICASSP)*, Seoul, Republic of Korea, 2024, pp. 8661–8665, doi: 10.1109/ICASSP48485.2024.10446001.

[34] C. Liu et al., "Low-complexity parameter learning for OTFS modulation based automotive radar," in *Proc. IEEE Int. Conf. Acoust. Speech Signal Process. (ICASSP)*, Toronto, ON, Canada, 2021, pp. 8208–8212, doi: 10.1109/ICASSP39728.2021.9414107.

[35] Z. Wei, W. Yuan, S. Li, J. Yuan, and D. W. K. Ng, "Off-grid channel estimation with sparse Bayesian learning for OTFS systems," *IEEE Trans. Wireless Commun.*, vol. 21, no. 9, pp. 7407–7426, 2022, doi: 10.1109/TWC.2022.3158616.

SP